

Exploring Cycle Consistency Learning in Interactive Volume Segmentation

Qin Liu¹, Meng Zheng², Benjamin Planche², Zhongpai Gao²,
Terrence Chen², Marc Niethammer¹, and Ziyang Wu²

¹ University of North Carolina at Chapel Hill

² United Imaging Intelligence, Cambridge MA, USA

<https://github.com/uncbiag/iSegFormer/tree/v2.0>

Abstract. Automatic medical volume segmentation often lacks clinical accuracy, necessitating further refinement. In this work, we interactively approach medical volume segmentation via two decoupled modules: *interaction-to-segmentation* and *segmentation propagation*. Given a medical volume, a user first segments a slice (or several slices) via the interaction module and then propagates the segmentation(s) to the remaining slices. The user may repeat this process multiple times until a sufficiently high volume segmentation quality is achieved. However, due to the lack of human correction during propagation, segmentation errors are prone to accumulate in the intermediate slices and may lead to sub-optimal performance. To alleviate this issue, we propose a simple yet effective cycle consistency loss that regularizes an intermediate segmentation by referencing the accurate segmentation in the starting slice. To this end, we introduce a backward segmentation path that propagates the intermediate segmentation back to the starting slice using the same propagation network. With cycle consistency training, the propagation network is better regularized than in standard forward-only training approaches. Evaluation results on challenging AbdomenCT-1K and OAI-ZIB datasets demonstrate the effectiveness of our method.

1 Introduction

Volumetric medical image segmentation is critical in various applications, ranging from disease diagnosis [1–4] to surgical planning and treatment [5, 6]. Automatic approaches often lack clinical accuracy, necessitating further corrections [7]. Interactive segmentation, which allows users to refine automated segmentations with additional hints (*e.g.*, clicks [8], scribbles [9], and bounding boxes [10]), appears to be an effective way for segmentation refinement. Therefore, we focus on interactive volume segmentation in this work.

Highly successful temporal propagation modules have been proposed for semi-supervised video object segmentation (VOS) [11–13]. Inspired by these approaches, recent interactive volume segmentation methods [14–16] have used a modular framework that decouples human interaction from segmentation propagation. In this way, a video temporal propagation module can be directly applied

to medical volumes. Conceptually, these modular methods combine two tasks: interaction-to-segmentation (*i.e.*, interactive segmentation on 2D slices [8]) and segmentation propagation (*i.e.*, as in temporal propagation in semi-supervised VOS [12]). These modular methods differ significantly from unified 3D approaches [17, 18], which directly adopt 3D encoders and decoders for interactive volume segmentation. Modular approaches, as opposed to unified ones, allow users to focus on segmenting a single slice with high quality without having to check the interaction effects on other slices, as checking itself takes time and effort. Besides, modular methods offer greater flexibility in supporting various user interactions since interaction and propagation are decoupled. In the era of large foundation models, modular methods benefit from the advances of both modules [19, 20]. Thus, we focus on modular interactive volume segmentation.

The propagation module in existing modular approaches [14–16] rely on the state-of-the-art Space Time Memory network (STM) [11] and Space Time Correspondence Network (STCN) [12]). STM builds a memory bank that stores representations for intermediate images and their segmentations. A query image retrieves a segmentation from this memory bank by the learned correspondence between query and memory representations. STCN improves STM by introducing a much more memory-efficient correspondence learning approach. STM and STCN use a sequential propagation order to support online video processing. This online restriction is unnecessary in medical volumes, typically acquired offline before segmentation. Moreover, segmentation errors can accumulate in intermediate slices without human correction, potentially degrading the memory bank and leading to suboptimal performance.

To alleviate this issue, we propose a simple yet effective cycle consistency loss that regularizes an intermediate segmentation by referencing an accurate segmentation in the starting slice. To this end, we introduce a backward segmentation path that propagates the intermediate segmentation back to the starting slice using the same propagation network. Compared with the propagated segmentation of intermediate slices, the segmentation of the starting slice is always accurate and reliable. Therefore, the accurate segmentation in the starting slice will alleviate the segmentation errors of an intermediate slice that is flowing in a forward-backward loop. We evaluated cycle consistency training on several public benchmarks, including AbdomenCT-1K [21] and OAI-ZIB [22]. Evaluation results on the AbdomenCT-1K dataset show that cycle consistency training improved segmentation on 8 out of 12 organs, including **24.9%** and **8.3%** improvements for the challenging esophagus and inferior vena cava, respectively.

Our contributions are as follows: 1) we investigate the error accumulation problem of existing propagation modules for interactive volume segmentation and mitigate it by better training regularization; 2) we explore a simple yet effective cycle consistency training strategy that encourages self-correction for the intermediate propagated segmentations; and 3) we demonstrate the effectiveness of our proposed method on challenging and diverse benchmarks. To the best of our knowledge, we are the first to explore cycle consistency learning in interactive volume segmentation.

2 Related Work

Video object segmentation (VOS). We focus on semi-supervised VOS that aims to segment a video object given the segmentation of the first frame [23]. We are particularly interested in approaches such as STM [11] and STCN [12] that build a memory bank for explicit pixel-level matching. STM was a breakthrough memory network that inspired many follow-up works such as SwiftNet [24] and STCN. Even though these memory networks were developed for videos, they have recently been applied for interactive segmentation on medical volumes [14–16]. However, all these methods have the inherent memory network limitation of accumulating propagation errors in an expanding memory bank. *In this work, we explore using cycle consistency learning to mitigate this problem for interactive volume segmentation.*

Interactive volume segmentation. Modular interactive volume segmentation approaches have been proposed in [14–16]. Mem3D [15] first applies STM [11] as the propagation network for interactive volume segmentation. It further proposes a quality assessment module to recommend the next slice for refinement. iSegFormer [14] uses STCN [12], an upgraded STM, as the propagation module and shows that the STCN model trained on videos can perform well on medical images even without finetuning. HybridNet [16] proposes a hybrid propagation network that combines STCN with a 3D encoder-decoder network to provide spatially consistent features, demonstrating these features’ effectiveness in improving interactive segmentation performance. *In this work, we use STCN as the propagation network due to its strong performance. Unlike previous methods, we focus on exploring cycle-consistent learning in interactive volume segmentation.*

Cycle consistency learning. Cycle consistency learning has been explored in various tasks such as video object segmentation [25], image synthesis [26], and unsupervised pretraining [27, 28]. Besides, it has been applied to medical image segmentation [29], registration [30–32], and synthesis [33]. *In this work, we explore cycle consistency learning in interactive volume segmentation. More specifically, we aim to address the error accumulation problem in the propagation module by regularizing intermediate segmentations via a cyclic mechanism.*

3 Cycle Consistency Learning

3.1 Problem Formulation

Given a volume with T slices, a memory slice m is defined as the starting slice for propagation; a query slice q is defined as the target slice to be propagated; an intermediate slice p is defined as any slice that locates between m and q . The ground truth segmentations of slices m , p , and q are denoted as m_gt , p_gt , and q_gt , respectively. A propagation network parameterized by θ is denoted as net_θ , which segments the intermediate slice as below:

$$p_seg = net_\theta(p, [m, m_gt]) \quad (1)$$

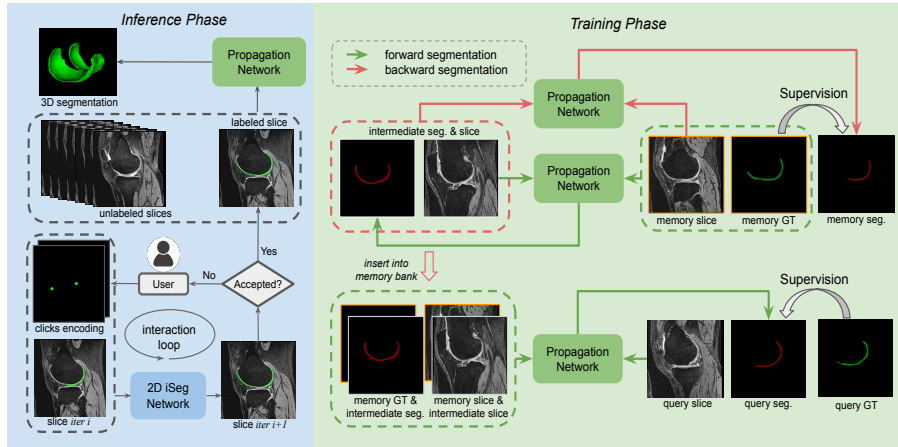


Fig. 1. Method overview. Left: our modular framework for interactive volume segmentation. Right: cycle-consistent training for the propagation module, in which all propagation networks share the weights. We introduce a backward segmentation path (shown in red arrows) into a standard training process that consists of only forward segmentation paths (shown in green arrows). “GT” denotes ground truth (shown in green); “seg.” denotes model segmentation (shown in red).

where $[\cdot]$ denotes a scalable memory bank that can be updated by appending more (slice, segmentation) pairs. For example, to segment the query slice, the memory bank may be updated as $[m, m_gt, p, p_seg]$ by appending the intermediate slice p and its segmentation p_seg .

3.2 Cycle Consistency Training

For cycle consistency training, we randomly sample three slices (*i.e.* a memory slice m , an intermediate slice p , and a query slice q as defined in Sec. 3.1). The ground truth segmentations of the three slices are also provided. Fig. 1 shows the process of training a propagation network net_θ (or net in short) via the three slices. In a nutshell, cycle consistency training introduces a backward segmentation path (shown in red arrows) into standard training that only performs forward segmentation (shown in green arrows). Next, we will introduce the details of forward and backward segmentation.

Forward segmentation. There are two stages in forward segmentation: 1) the first stage propagates the memory ground truth m_gt to the intermediate slice p , resulting in an intermediate segmentation p_seg . This stage is denoted as $p_seg = net(p, [m, m_gt])$, in which the memory bank $[m, m_gt]$ only contains a memory slice and its ground truth. 2) the query slice then retrieves a segmentation via an updated memory bank $[m, m_gt, p, p_seg]$, which leverages the intermediate segmentation. This stage is denoted as $q_seg = net(q, [m, m_gt, p, p_seg])$.

Algorithm 1: Pseudocode for calculating cycle consistency loss

```

# net: propagation network with learnable parameters
# loss: segmentation loss function (e.g., cross-entropy loss)
# lambda: loss weight
# m, p, q: memory, intermediate, and query slices
# m_gt, q_gt: ground truths for memory and query slices

# forward segmentation
p_seg, q_seg = net(p, [m, m_gt]), net(q, [m, m_gt, p, p_seg])

# backward segmentation
m_seg = net(m, [p, p_seg])

# cycle loss
q_loss, m_loss = loss(q_seg, q_gt), loss(m_seg, m_gt)
cycle_loss = q_loss + lambda * m_loss

```

Backward segmentation. To further regularize the intermediate segmentation p_seg obtained in forward segmentation, we propagate the intermediate segmentation p_seg back to the memory slice m using the same propagation network net . Thus, we obtain m_seg and complete a propagation loop. The backward segmentation path can be denoted as $m_seg = net(m, [p, p_seg])$.

3.3 Cycle Consistency Loss

Alg. 1 shows the pseudo-code for obtaining the cycle consistency loss. Given the segmentations from the forward and backward paths (described in Sec. 3.2), we define cycle consistency loss \mathcal{L}_{cycle} as

$$\mathcal{L}_{cycle} = \mathcal{L}(q_seg, q_gt) + \lambda \mathcal{L}(m_seg, m_gt) \quad (2)$$

where \mathcal{L} denotes a conventional segmentation loss and $\lambda \geq 0$ is a weight for the memory segmentation loss. The query segmentation q_seg and the memory segmentation m_seg are supervised by their corresponding ground truths using the same loss function \mathcal{L} . The intermediate segmentation p_seg can also be supervised by its ground truth, but we ignore this loss in Eq. 2 for brevity. When $\lambda = 0$, our cycle consistency loss degrades to the standard loss.

3.4 Implementation Details

Networks. For the propagation network, we use a video-pretrained STCN [12] as the baseline and fine-tune it on medical images with or without the proposed cycle consistency loss. STCN consists of a key encoder and a value encoder using ResNet50 and ResNet18, respectively. For the 2D interactive segmentation network, any existing open-source method [8, 19, 34] can be combined with STCN for interactive volume segmentation. This network is not the focus of our work and is only used in qualitative evaluation (see demos in the appendix).

Training. We set $\lambda = 0.1$ in the cycle consistency loss based on parameter tuning on video datasets (Sec. 4.3). We adopt most of the hyperparameters introduced in STCN [12] for a fair comparison with the baseline. For example, we follow the same data augmentation strategy that randomly reverses the order of the slices in a training batch; we also use bootstrapped cross entropy as the segmentation loss in Alg. 1 and Eq. 2. Our implementation is based on Python and PyTorch. Our models are trained and evaluated on an NVIDIA RTX A6000 GPU. We fix the number of finetuning iterations to 10k without model selection.

4 Experiments

4.1 Benchmarks

Datasets. We evaluate our method on two datasets: AbdomenCT-1K [21] and OAI-ZIB [22]. **AbdomenCT-1K** contains 50 CT abdomen volumes (4794 slices) with manual segmentations for 12 diversified organs (Fig. 2), including tiny and challenging organs such as the pancreas and esophagus, as well as large and regular organs such as the liver and kidney. Our experiments leverage large-scale, video-pretrained weights for the propagation model, requiring minimal data for fine-tuning and allocating the bulk of the data for evaluation. This experiment setting mirrors the scarcity of annotated medical volumes. We randomly partitioned the AbdomenCT-1K dataset into 10 volumes (955 slices) for fine-tuning and 40 volumes (3839 slices) for testing, utilizing all 12 organs in both phases. Consequently, these organs are classified as “seen” organs. We also generate rib segmentations for the testing volumes to evaluate the model’s generalizability and use them as “unseen” organs. We generate rib segmentations using our internally developed rib segmentation model with minor manual refinement (an example is shown in the appendix). **OAI-ZIB** consists of 507 3D MR images with segmentations for the femur, tibia, tibial cartilage, and femoral cartilage. In this work, we only conduct a qualitative evaluation using this dataset.

Evaluation protocol. For *quantitative* evaluation, we only conduct one round of propagation for simplicity and efficiency; we evaluate each organ separately and use the ground truth for propagation to decouple the interaction module. We follow the same propagation strategy introduced in STCN [12]. For *qualitative* evaluation, we conduct multiple rounds of propagation and rely on the interaction module to provide the first segmentation and refine propagation results.

Evaluation metrics. We report Region Jaccard (\mathcal{J}), Boundary F measure (\mathcal{F}), and their average ($\mathcal{J}\&\mathcal{F}$) to assess segmentation quality. We also report the Dice Similarity Coefficient (DSC) as an additional metric.

4.2 Comparisons

Baselines. We use two popular video object segmentation models, STM [11] and STCN [12], as the baselines. The baselines are pretrained on videos. We finetune STCN on medical datasets w/ and w/o cycle consistency loss. See Tab. 1 for comparisons.

	AbdomenCT-1K				Left Rib (unseen)				Right Rib (unseen)			
	\mathcal{J}	\mathcal{F}	$\mathcal{J}\&\mathcal{F}$	DSC	\mathcal{J}	\mathcal{F}	$\mathcal{J}\&\mathcal{F}$	DSC	\mathcal{J}	\mathcal{F}	$\mathcal{J}\&\mathcal{F}$	DSC
STM [11]	31.4	39.8	35.6	47.8								
STCN [12]	56.0	74.3	66.1	71.8	27.4	45.2	36.3	43.0	23.3	36.9	30.1	37.8
+FT w/o cycle	64.9	82.4	74.7	78.7	38.3	59.0	48.7	55.4	33.9	57.0	45.4	50.6
+FT w/ cycle	66.8	85.1	76.9	80.1	41.0	64.6	52.8	58.2	35.6	60.7	48.2	52.5

Table 1. Quantitative comparisons of our method and baselines on AbdomenCT-1K [21]. We observe significant improvement when finetuning the SOTA video-pretrained STCN model on medical images with our proposed cycle consistency loss.

Quantitative comparisons. Tab. 1 shows quantitative comparison results on the AbdomenCT-1K dataset. We compare three models: 1) a baseline STCN model that was pretrained on videos without being finetuned on AbdomenCT-1K; 2) a finetuned baseline model without the cycle consistency learning; 3) a finetuned baseline model with cycle consistency learning. In addition to the 12 labeled organs (*i.e.*, “seen” organs), we generate the segmentations of ribs (*i.e.*, “unseen” organs) for the testing volumes to evaluate a model’s generalizability. All results in Tab. 1 are averaged over all volumes and all organs. First, we observe that finetuning an STCN model on medical images can significantly improve its performance. Second, our results show that cycle consistency learning can further boost the model’s performance, for both seen and unseen organs, demonstrating the benefits of our method. The relative improvement for each organ is shown in Fig. 2.

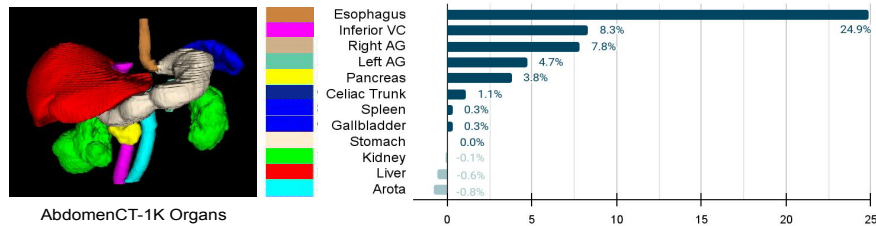


Fig. 2. Relative $\mathcal{J}\&\mathcal{F}$ improvement on the AbdomenCT-1K dataset. Although the performance drops slightly for 3 organs, we observe improvements on 8 out of the full set of 12 organs, resulting in average improvements across all metrics (Tab. 1).

Qualitative comparisons. We compare our method (FT w/ cycle) with our baseline (FT w/o cycle) in Fig. 3. As the ground truth for the Aorta (light blue) is not fully annotated at the top, our cycle consistency loss shows lower performance on the Aorta (Fig. 2) because it extends it beyond the annotation.

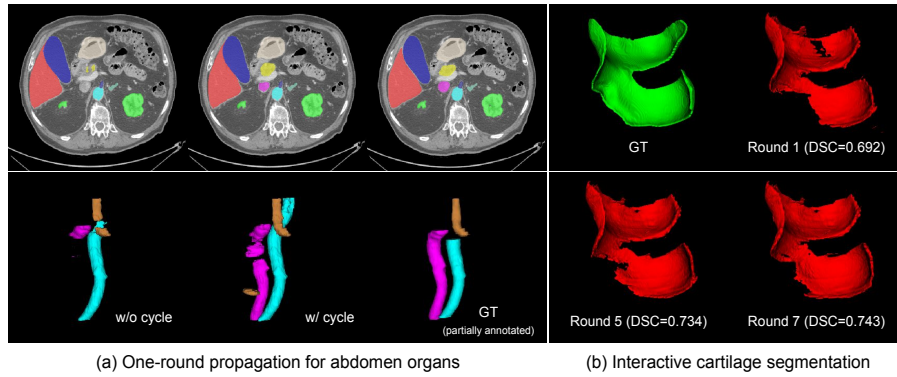


Fig. 3. Qualitative comparison of our method and baseline on *AbdomenCT-1K* [21] and *OAI-ZIB* [22]. With cycle consistency learning, the STCN model achieves better performance for abdomen vessel segmentation.

4.3 Ablations

We performed ablations on video datasets to obtain the best λ . We finetuned an STCN baseline on the training set of YouTubeVOS 2018 [35] with different values for λ . Evaluation results of the validation set show that $\lambda = 0.1$ achieves the best performance; this is the value we used for our experiments in Tab. 1.

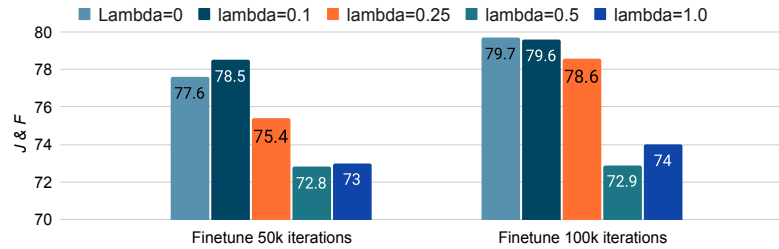


Fig. 4. Ablation study on YouTubeVOS 2018 [35]. $\lambda = 0.1$ achieves the best result.

5 Conclusion

We explored cycle consistency learning for interactive volume segmentation, aiming to address the pervasive error accumulation issue plaguing propagation modules. By introducing a segmentation backward path and integrating a cycle consistency loss, we seamlessly wove these advancements into current methodologies for medical volume segmentation. The efficacy of our strategy was rigorously affirmed through evaluations on challenging benchmarks, paving the road for developing more capable and advanced methods in the field.

References

1. D. Shen, G. Wu, and H.-I. Suk, “Deep learning in medical image analysis,” *Annual review of biomedical engineering*, vol. 19, pp. 221–248, 2017. **1**
2. G. Litjens, T. Kooi, B. E. Bejnordi, A. A. A. Setio, F. Ciompi, M. Ghafoorian, J. A. Van Der Laak, B. Van Ginneken, and C. I. Sánchez, “A survey on deep learning in medical image analysis,” *MedIA*, vol. 42, pp. 60–88, 2017. **1**
3. S. Devunooru, A. Alsadoon, P. Chandana, and A. Beg, “Deep learning neural networks for medical image segmentation of brain tumours for diagnosis: a recent review and taxonomy,” *Journal of Ambient Intelligence and Humanized Computing*, vol. 12, pp. 455–483, 2021. **1**
4. T. Heimann, B. J. Morrison, M. A. Styner, and M. Niethammer, “Segmentation of knee images: a grand challenge,” **1**
5. J. Li, M. Erdt, F. Janoos, T.-c. Chang, and J. Egger, “Medical image segmentation in oral-maxillofacial surgery,” *Computer-Aided Oral and Maxillofacial Surgery*, pp. 1–27, 2021. **1**
6. L. Soler, H. Delingette, G. Malandain, J. Montagnat, N. Ayache, C. Koehl, O. Dourthe, B. Malassagne, M. Smith, D. Mutter, *et al.*, “Fully automatic anatomical, pathological, and functional segmentation from CT scans for hepatic surgery,” *Computer Aided Surgery*, vol. 6, no. 3, pp. 131–142, 2001. **1**
7. G. Wang, W. Li, M. A. Zuluaga, R. Pratt, P. A. Patel, M. Aertsen, T. Doel, A. L. David, J. Deprest, S. Ourselin, *et al.*, “Interactive medical image segmentation using deep learning with image-specific fine tuning,” *IEEE TMI*, vol. 37, no. 7, pp. 1562–1573, 2018. **1**
8. Q. Liu, Z. Xu, G. Bertasius, and M. Niethammer, “SimpleClick: Interactive image segmentation with simple vision transformers,” *arXiv:2210.11006*, 2022. **1, 2, 5**
9. H. K. Cheng, Y.-W. Tai, and C.-K. Tang, “Modular interactive video object segmentation: Interaction-to-mask, propagation and difference-aware fusion,” in *CVPR*, pp. 5559–5568, 2021. **1**
10. S. Zhang, J. H. Liew, Y. Wei, S. Wei, and Y. Zhao, “Interactive object segmentation with inside-outside guidance,” in *CVPR*, pp. 12234–12244, 2020. **1**
11. S. W. Oh, J.-Y. Lee, N. Xu, and S. J. Kim, “Video object segmentation using space-time memory networks,” in *CVPR*, pp. 9226–9235, 2019. **1, 2, 3, 6, 7**
12. H. K. Cheng, Y.-W. Tai, and C.-K. Tang, “Rethinking space-time networks with improved memory coverage for efficient video object segmentation,” *NeurIPS*, vol. 34, pp. 11781–11794, 2021. **1, 2, 3, 5, 6, 7**
13. H. K. Cheng and A. G. Schwing, “XMem: Long-term video object segmentation with an Atkinson-Shiffrin memory model,” in *ECCV*, pp. 640–658, 2022. **1**
14. Q. Liu, Z. Xu, Y. Jiao, and M. Niethammer, “isegformer: Interactive segmentation via transformers with application to 3D knee MR images,” in *MICCAI*, pp. 464–474, 2022. **1, 2, 3**
15. T. Zhou, L. Li, G. Bredell, J. Li, J. Unkelbach, and E. Konukoglu, “Volumetric memory network for interactive medical image segmentation,” *MedIA*, vol. 83, p. 102599, 2023. **1, 2, 3**
16. L. Shi, X. Zhang, Y. Liu, and X. Han, “A hybrid propagation network for interactive volumetric image segmentation,” in *MICCAI*, pp. 673–682, 2022. **1, 2, 3**
17. A. Diaz-Pinto, P. Mehta, S. Alle, M. Asad, R. Brown, V. Nath, A. Ihsani, M. Antonelli, D. Palkovics, C. Pinter, *et al.*, “DeepEdit: Deep editable learning for interactive segmentation of 3D medical images,” in *MICCAI Workshop on Data Augmentation, Labelling, and Imperfections (DALI)*, pp. 11–21, 2022. **2**

18. X. Liao, W. Li, Q. Xu, X. Wang, B. Jin, X. Zhang, Y. Wang, and Y. Zhang, "Iteratively-refined interactive 3d medical image segmentation with multi-agent reinforcement learning," in *CVPR*, pp. 9394–9402, 2020. [2](#)
19. A. Kirillov, E. Mintun, N. Ravi, H. Mao, C. Rolland, L. Gustafson, T. Xiao, S. Whitehead, A. C. Berg, W.-Y. Lo, *et al.*, "Segment anything," *arXiv preprint arXiv:2304.02643*, 2023. [2](#), [5](#)
20. H. K. Cheng, S. W. Oh, B. Price, J.-Y. Lee, and A. Schwing, "Putting the object back into video object segmentation," in *arXiv*, 2023. [2](#)
21. J. Ma, Y. Zhang, S. Gu, C. Zhu, C. Ge, Y. Zhang, X. An, C. Wang, Q. Wang, X. Liu, S. Cao, Q. Zhang, S. Liu, Y. Wang, Y. Li, J. He, and X. Yang, "AbdomenCT-1K: Is abdominal organ segmentation a solved problem?," *IEEE TPAMI*, 2021. [2](#), [6](#), [7](#), [8](#)
22. F. Ambellan, A. Tack, M. Ehlke, and S. Zachow, "Automated segmentation of knee bone and cartilage combining statistical shape knowledge and convolutional neural networks: Data from the osteoarthritis initiative," *MedIA*, vol. 52, pp. 109–118, 2019. [2](#), [6](#), [8](#)
23. M. Gao, F. Zheng, J. J. Yu, C. Shan, G. Ding, and J. Han, "Deep learning for video object segmentation: a review," *Artificial Intelligence Review*, vol. 56, no. 1, pp. 457–531, 2023. [3](#)
24. H. Wang, X. Jiang, H. Ren, Y. Hu, and S. Bai, "Swiftnet: Real-time video object segmentation," in *CVPR*, pp. 1296–1305, 2021. [3](#)
25. Y. Li, N. Xu, J. Peng, J. See, and W. Lin, "Delving into the cyclic mechanism in semi-supervised video object segmentation," *NeurIPS*, vol. 33, pp. 1218–1228, 2020. [3](#)
26. J.-Y. Zhu, T. Park, P. Isola, and A. A. Efros, "Unpaired image-to-image translation using cycle-consistent adversarial networks," in *ICCV*, pp. 2223–2232, 2017. [3](#)
27. D. Dwibedi, Y. Aytar, J. Tompson, P. Sermanet, and A. Zisserman, "Temporal cycle-consistency learning," in *CVPR*, pp. 1801–1810, 2019. [3](#)
28. X. Wang, A. Jabri, and A. A. Efros, "Learning correspondence from the cycle-consistency of time," in *CVPR*, pp. 2566–2576, 2019. [3](#)
29. R. Wang and G. Zheng, "CyCMIS: Cycle-consistent cross-domain medical image segmentation via diverse image augmentation," *MedIA*, vol. 76, p. 102328, 2022. [3](#)
30. B. Kim, D. H. Kim, S. H. Park, J. Kim, J.-G. Lee, and J. C. Ye, "CycleMorph: cycle consistent unsupervised deformable image registration," *MedIA*, vol. 71, p. 102036, 2021. [3](#)
31. H. Greer, R. Kwitt, F.-X. Vialard, and M. Niethammer, "ICON: Learning regular maps through inverse consistency," in *CVPR*, pp. 3396–3405, 2021. [3](#)
32. L. Tian, H. Greer, F.-X. Vialard, R. Kwitt, R. S. J. Estépar, and M. Niethammer, "GradICON: Approximate diffeomorphisms via gradient inverse consistency," *arXiv preprint arXiv:2206.05897*, 2022. [3](#)
33. C. Wang, G. Macnaught, G. Papanastasiou, T. MacGillivray, and D. Newby, "Un-supervised learning for cross-domain medical image synthesis using deformation invariant cycle consistency networks," in *MICCAI Workshop on Simulation and Synthesis in Medical Imaging (SASHIMI)*, pp. 52–60, 2018. [3](#)
34. X. Zou, J. Yang, H. Zhang, F. Li, L. Li, J. Wang, L. Wang, J. Gao, and Y. J. Lee, "Segment everything everywhere all at once," *Advances in Neural Information Processing Systems*, vol. 36, 2024. [5](#)
35. N. Xu, L. Yang, Y. Fan, D. Yue, Y. Liang, J. Yang, and T. Huang, "Youtube-vos: A large-scale video object segmentation benchmark," *arXiv preprint arXiv:1809.03327*, 2018. [8](#)